A&A 439, 635–643 (2005)
DOI: 10.1051/0004-6361:20042248

Astronomy & Astrophysics

TeV gamma-ray observations of SS-433 and a survey of the surrounding field with the HEGRA IACT-System

F. Aharonian[1], A. Akhperjanian[7], M. Beilicke[4], K. Bernlöhr[1], H.-G. Börst[5], H. Bojahr[6], O. Bolz[1], T. Coarasa[2], J. Contreras[3], J. Cortina[10], S. Denninghoff[2], V. Fonseca[3], M. Girma[1], N. Götting[4], G. Heinzelmann[4], G. Hermann[1], A. Heusler[1], W. Hofmann[1], D. Horns[1], I. Jung[1,9], R. Kankanyan[1], M. Kestel[2], A. Kohnle[1], A. Konopelko[1,14], D. Kranich[2], H. Lampeitl[4], M. Lopez[3], E. Lorenz[2], F. Lucarelli[3], O. Mang[5], D. Mazin[2], H. Meyer[6], R. Mirzoyan[2], A. Moralejo[3], E. Oña-Wilhelmi[3], M. Panter[1], A. Plyasheshnikov[1,8], G. Pühlhofer[11], R. de los Reyes[3], W. Rhode[6], J. Ripken[4], G. P. Rowell[1], V. Sahakian[7], M. Samorski[5], M. Schilling[5], M. Siems[5], D. Sobzynska[2,12], W. Stamm[5], M. Tluczykont[4,13], V. Vitale[2], H. J. Völk[1], C. A. Wiedner[1], and W. Wittek[2]

[1] Max-Planck-Institut für Kernphysik, Postfach 103980, 69029 Heidelberg, Germany, e-mail: Gavin.Rowell@mpi-hd.mpg.de; [2] Max-Planck-Institut für Physik, Föhringer Ring 6, 80805 München, Germany; [3] Universidad Complutense, Facultad de Ciencias Físicas, Ciudad Universitaria, 28040 Madrid, Spain; [4] Universität Hamburg, Institut für Experimentalphysik, Luruper Chaussee 149, 22761 Hamburg, Germany; [5] Universität Kiel, Inst. f. Experimentelle und Angewandte Physik, Leibnizstr. 15-19, 24118 Kiel, Germany; [6] Universität Wuppertal, Fachbereich Physik, Gaußstr.20, 42097 Wuppertal, Germany; [7] Yerevan Physics Institute, Alikhanian Br. 2, 375036 Yerevan, Armenia; [8] Altai State University, Dimitrov Street 66, 656099 Barnaul, Russia; [9] Now at Washington University, St. Louis MO 63130, USA; [10] Now at Max-Planck-Institut für Physik, Föhringer Ring 6, 80805 München, Germany; [11] Now at Landessternwarte Heidelberg, Königstuhl, Heidelberg, Germany; [12] Home institute: University Lodz, Poland; [13] Now at Laboratoire Leprince-Ringuet, École Polytechnique, Palaiseau, France (IN2P3/CNRS); [14] Now at Humboldt Universität f. Physik, Newtonstr. 15, Berlin, Germany

Received 25 October 2004 / Accepted 28 March 2005

Abstract. We present results of a search for TeV γ-ray emission from the microquasar SS-433 and the surrounding region covering a $\sim 8^\circ \times 8^\circ$ field of view. Analysis of data taken with the HEGRA stereoscopic system of imaging atmospheric Čerenkov imaging telescopes reveals no evidence of steady or variable emission from any position. Observation times of over 100 h have been achieved in central parts of the field of view. We set 99% confidence level upper limits to a number of a-priori-chosen objects of interest, including SS-443 and its interaction regions, 32 pulsars, 3 supernova remnants and the GeV source GeV J1907+0537. Our upper limit of 3.2% Crab flux (for energies $E > 0.8$ TeV) for the eastern-lobe region *e3* of SS-433 permits, after comparison with X-ray fluxes, a lower limit of $B \geq 19\ \mu$G on the post-shocked magnetic field in this region. An ensemble upper limit at 0.3% Crab flux ($E > 0.7$ TeV) from a subset (11) of the 32 pulsars implies a maximum of 4.5% of the spin-down pulsar power is available for TeV γ-ray production. For one of the SNR in our FoV, 3C 396, recent Chandra observations suggest that a central pulsar-driven wind nebula may be the source of X-ray emission. Our upper limit implies that a maximum of 0.1% of the spin-down power from the central source of 3C 396 would be available for TeV γ-rays.

Key words. gamma rays: observations – stars: individual: SS-433

1. Introduction

SS-433 is the first, and best-known microquasar (Mirabel & Rodríguez 1999) powered by a compact object (neutron star or black hole), which in turn drives a bi-polar jet. The companion star, possibly a Wolf-Rayet (Fuchs et al. 2002), is in a 13 day orbit with the compact object. The bi-polar jet with a bulk speed of $0.26c$ (Margon et al. 1981) precesses with a ~162.5 day period and is oriented at an angle ~79° to the line of sight. The morphology of the associated supernova remnant (SNR) W50, is likely heavily influenced by the jet pressure imparted on the surrounding interstellar medium. Observations at TeV γ-ray energies of SS-433 and surroundings are motivated by the extraordinary kinetic *quiescent* power output of the jets in the range 10^{39} to 10^{41} erg s^{-1} (Margon 1984; Kawai & Kotani 1999; Safi-Harb & Ögelman 1997). This output amounts to a reasonable fraction of that required to maintain the Galactic cosmic-ray (CR) flux which is a few $\times\ 10^{41}$ erg s^{-1} (Blandford 1980). SS-433/W50, at a distance of 5.5 kpc (Vermeulen et al. 1993), may therefore be one of the most powerful, and indeed most significant sites of CR acceleration in our Galaxy. Observations at TeV γ-ray energies provide important constraints on the likelihood of this scenario, and also on the conversion efficiency of kinetic energy into accelerated particles.

The framework described by Aharonian & Atoyan (1998), hereafter AA, suggests that an appreciable flux of TeV γ-rays

from SS-433 may be observed by ground-based γ-ray instruments. Inverse-Compton scattering of cosmic microwave background (CMB) photons by electrons accelerated at the eastern jet termination shock ~60′ east of SS-433 will result in a TeV γ-ray flux. This termination shock region is termed *e3* (Safi-Harb & Ögelman 1997) or the "radio ear" by Dubner et al. (1998) (see Fig. 1). The *e3* location is likely an interaction region of the eastern jet particles and interstellar medium (ISM), and may contain a non-relativistic shock of the type suggested in shell-type SNR. A rather steep power law ($F_x \propto E^{-\Gamma}$; $\Gamma = 3.7^{+2.3}_{-0.7}$) describes well the *e3* X-ray emission, although a thermal Bremsstrahlung interpretation for the X-ray emission is presently not ruled out due to the limiting energy resolution of ASCA and ROSAT (Safi-Harb & Ögelman 1997). The spatial correlation however between the radio and X-ray emission (Brinkmann et al. 1996; Dubner et al. 1998) at *e3* is strong circumstantial evidence in favour of a non-thermal interpretation. Actually, a strong radio/X-ray correlation is noticed only for the *e3* region, with other positions along the jet less prominent at radio energies. If the X-rays at *e3* are indeed due to synchrotron emission, we can conclude that electrons there are accelerated to Multi-TeV energies. At other regions along the eastern jet non-thermal mechanisms for the X-ray emission such as inverse-Compton, synchrotron-self-Compton (Band & Grindlay 1986) and synchrotron emission (Safi-Harb & Petre 1999) have been invoked. A general hardening of the X-ray power-law spectral index is noticed as one progresses along the eastern jet closer to SS-433 itself. The western jet is more prominent at radio and infrared (IR) wavelengths, exhibiting broad-scale (>10 arcmin) correlation and small-scale IR knots (Fuchs 2002). Knots are also seen in X-rays (ASCA and ROSAT) but do not in general correlate with those found in the IR bands. Correlation is also seen between some prominent IR knots (labelled knot2 and knot3 by Fuchs (2002) and radio emission at the CO(1–0) line (2.6 mm), suggesting interaction with local, dense molecular clouds. It is unclear if the IR emission is thermal or non-thermal. The higher density of ambient matter in the western region might be favourable conditions for TeV γ-ray emission from the interaction of accelerated hadrons ($p + p \rightarrow \pi^\circ + X \rightarrow 2\gamma$).

Observations at TeV energies can play a vital role in validating the synchrotron/inverse-Compton (S/IC) framework since the TeV γ-ray (f_γ) and X-ray (f_x) energy fluxes (above γ-ray energies E and X-ray energies ϵ respectively) are linked accordingly for IC scattering on the cosmic microwave background (CMB): in both X and γ-rays (Aharonian et al. 1997):

$$\frac{\xi\, f_x(\geq \epsilon \text{ keV})}{f_\gamma(\geq E \text{ TeV})} \sim 10 \left(\frac{B}{10^{-5} \text{ G}} \right)^2 \quad (1)$$

so that the shock-compressed magnetic field B can be determined explicitly, thus providing important information on particle acceleration properties. The filling factor $\xi \geq 1.0$ allows for emission regions of different sizes at X-ray and γ-ray energies. This can result if electrons escape/diffuse to regions of different B field from that of their corresponding synchrotron photons. Corresponding energies for the above comparison arise from S/IC theory such that the X-ray photon energy is related to the TeV γ-ray photon of energy E:

$$\epsilon \sim 0.07 (E/1 \text{ TeV}) \left(B/10^{-5} \text{ G} \right) \text{ keV}. \quad (2)$$

At γ-ray energies $E \sim 1$ TeV a comparison of the X-ray energy flux at $\epsilon \sim 0.1$ keV is required for reasonable values of $B \sim 10$ to 100 μG expected after shock compression.

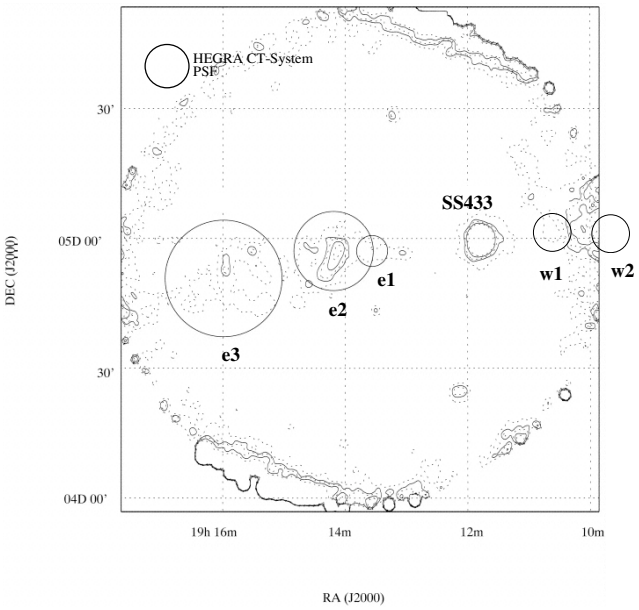

Fig. 1. ROSAT PSPC image (0.1 to 2.4 keV) concentrating on the eastern side of SS-433/W50. A number of areas are defined (*e1, e2, e3, w1, w2*) where separate spectral X-ray analyses were performed (Safi-Harb & Ögelman 1997). A circle is included depicting the point spread function (radius = 0.1°) of the HEGRA IACT-System. The large ring of radius ~2° is an instrument artifact.

Earlier results at TeV energies for SS-433 by the HEGRA IACT-System have been reported (Aharonian et al. 2002; Rowell et al. 2000, 2001). Upper limits for SS-433 and associated objects at energies at the 99% confidence level in the range 8 to 12% Crab flux were set. Interpreting the upper limit for the *e3* region (with radius 0.25°) at 2.1×10^{-12} ph cm^{-2} s^{-1} (0.13 Crab units) in the S/IC framework described above resulted in a *lower limit* on the *e3* magnetic field of $B \geq 13\,\mu$G. This TeV flux upper limit lies close to the prediction of AA, when assuming reasonable values for the size of *e3* (0.25° radius), electron injection power (10^{38} erg s^{-1}) and spectral index (−2). Recent preliminary results from CANGAROO-II (Hayashi et al. 2003) after 52 h exposure also yielded upper limits for SS-433 and environs.

The ~8° × 8° FoV achieved with all HEGRA IACT-System data also permits a wide survey for new TeV sources. In addition to the SS-433-related sources discussed above, a number of other a-priori chosen positions, corresponding to previously-identified sources were also chosen as potential sources of TeV emission. These included 23 pulsars, three SNR and one unidentified EGRET GeV source. Exposures of over 100 h in central parts of the FoV were achieved. For some of these sources, our upper limits can provide useful constraints on models of TeV γ-ray production.

2. Data & analysis

Data were collected using the HEGRA IACT-System[1], a group of 5 atmospheric Čerenkov telescopes which operated in coincidence for the detection of TeV γ-ray emission. Each telescope employed a multi-pixel camera of 271 photomultiplier tubes (PMTs) to view the generally elliptical images of extensive air shower (EAS) Čerenkov radiation initiated by γ-rays (and cosmic-rays) at the top of the atmosphere. The IACT-System operated at the Roque de los Muchachos, La Palma (2200 m asl, 28° 45′N 17° 54′W), until its decommissioning in September 2002. Full details of the IACT-System and its performance history can be found in Pühlhofer et al. (2003). The coincident trigger ensured a minimum trigger multiplicity of $n_{\rm tel} = 2$ telescopes view each EAS, and permitted the use of stereoscopic techniques. For each image, parameters such as *width*, *length*, *size*, *dis* are calculated using the well-known method of Hillas (1985), and are used to characterise the image's location, orientation and shape. Such characteristics from the ≥2 images per event form the basis of the stereoscopic approach used here, which yields accurate reconstruction of an event's arrival direction and its conformity to a true γ-ray event.

The ground-based detection of γ-rays must be made against a dominating isotropic background of cosmic-ray-initiated EAS. This background can be suppressed by exploiting the physical differences in EAS development between γ-ray and CRs, leading to differences in image shapes. A cut on the so-called *mean-scaled-width* parameter $\bar{w} = \sum_i^n width_i/(\langle w\rangle_i n)$, for n images (Aharonian et al. 2000), is used to reject CR images according to shape. Here, Monte-Carlo simulations are used to determine the expected width $\langle w\rangle$ for a true γ-ray, as a function of the image's *size*, impact parameter (distance of the EAS core from the telescope), and zenith angle of observations. The average of these so-called scaled widths $width_i/(\langle w\rangle_i)$ is then calculated to form $\bar{w}$. The distribution of $\bar{w}$ for true γ-rays is centred on unity with CR background events filling higher values (reflecting the higher fluctuations and nucleonic components in CR EAS).

Event arrival directions are calculated using the algorithms described by Hofmann et al. (1999) and yield an angular resolution better than 0.1° event-by-event, dependant upon the trigger multiplicity and energy of the event. The angular resolution is defined here as the standard deviation of a Gaussian fit to a point source of γ-rays (i.e. the point spread function, PSF). A cut on the parameter θ, the angular difference between the assumed and reconstructed arrival directions provides CR rejection based on direction. We have found that so-called "tight cuts", $\bar{w} < 1.1$ and $\theta_{\rm cut} < 0.12°$ are optimal for point-like sources in a background-dominated regime. In this analysis we primarily employed the direction reconstruction method described as "algorithm 3" by Hofmann et al. (1999), along with a minimum telescope trigger multiplicity of $n_{\rm tel} \geq 3$. Results from a number of γ-ray sources of the HEGRA IACT-System archive have found that removal of the exclusive $n_{\rm tel} = 2$ events yields better sensitivity. Similar results were also obtained using the other two direction reconstruction algorithms "1" and "2" as a check.

[1] High Energy Gamma Ray Astrophysics Imaging Atmospheric Čerenkov Telescope System.

Table 1. Selection criteria applied to data for run, image and event selection. Description of various parameters are as follows; *size*: total photoelectron yield in an image; *dis*: image centroid to camera centre distance. This cut is used to remove images truncated by the camera edge and their residual effects; $\bar{w}$: mean-scaled-width; $n_{\rm tel}$: number of telescope images used in stereo reconstruction and $\bar{w}$ calculation; *core*: distance from the central telescope (CT3) to the reconstructed shower core.

Run Selection	Trigger rate	≥0.75 Expected rate
Image Selection	Defective pixels	<15
	size	>40 photoelectrons
	dis	<1.7°
Dir. recons.		alg. "1", "2", "3"
Event Selection	$n_{\rm tel}$	≥3
	core	≤1000 m
	$\bar{w}$	<1.1
pt. source	$\theta_{\rm cut}$	<0.12°
extend. source		$< \sqrt{\theta_s^2 + 0.12^2}$
Background model		*template* model
		$1.3 < \bar{w} < 1.5$
		+ comparisons with other models

Observations analysed here represent all HEGRA IACT-System data with coverage of the SS-433 region, and utilised a total of 29 different tracking positions. The tracking positions were configured primarily under the so-called *wobble* mode in which a declination offset of ±0.5° with respect to a particular source of interest was applied. Some data however were also taken as part of an ON-OFF pair for which only the ON runs were considered, and also selected runs were taken from the HEGRA galactic plane scan (Aharonian et al. 2002). Table 1 summarises the various run, image and event selection criteria (the last one is described above). To remove data affected by adverse weather conditions, runs were selected if their raw trigger rate (from CR) was within a factor 0.75 of that expected for a given zenith angle, system configuration and epoch. A total of 391 runs were accepted for analysis reaching an exposure in excess of 100 h in central parts of the field of view (FoV) (see Table 2). Good image quality was maintained by rejecting images too close to the camera edge where they are distorted ($dis \geq 1.7°$) and also those strongly influenced by skynoise ($size \leq 40$ photoelectrons). The tracking positions for these data are scattered over a radius of a few degrees centred west of SS-433. Data were taken over 4 years in dedicated campaigns on SS-433, the SNR 3C 396 (SNR 039.2−00.3) and a scan of the galactic plane. Since the FoV response of single pointings has a rather wide $FWHM \sim 3.0°$, a combined analysis permits a search for TeV emission from potential sources over the FoV. The effective exposure (the product of the

Table 2. Summary of HEGRA IACT-System observations analysed here and passing run selection criteria of Table 1. The exposures refer to a region centred on SS-433 of diameter 4.0°.

Data subset	Obs. time (h)	Number of runs
1998	16.1	48
1999	54.6	212
2000	21.9	75
2001	16.4	56
Total	**109.9**	391

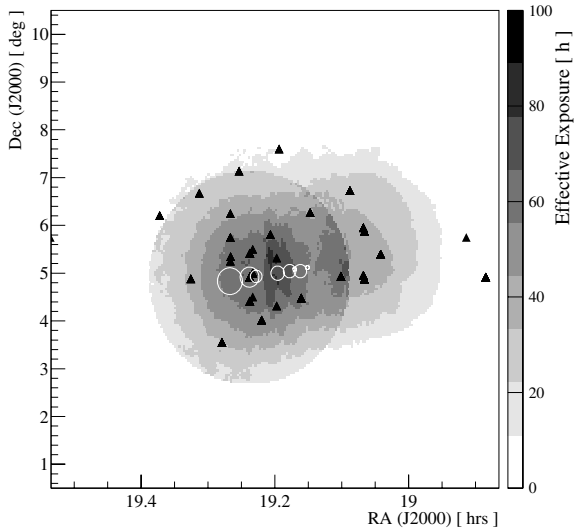

Fig. 2. Effective exposure ηt [h] achieved over the FoV for combined data. Here, η is the FoV response efficiency relative to a value unity at each tracking position, and t is the observation time. Tracking positions (a total of 29) are depicted by the black filled triangles. White circles overlaid represent a-priori targets associated with SS-433 (see Sect. 3).

FoV efficiency η and exposure t) over the FoV is shown in Fig. 2. η is estimated from the radial profile of γ-ray like events in the entire FoV (i.e. after the cut $\bar{w} < 1.1$), and agrees well with Monte-Carlo-derived efficiencies for true off-axis γ-rays.

3. Search for TeV sources

Guided by multiwavelength results, a number of regions in the FoV were chosen a-priori as possible sites of TeV γ-ray emission. These included those associated with the SS-433/W50 complex, a number of pulsars, and also SNRs. Where an extended source of radius θ_s is assumed, the cut on event direction used in this analysis, θ_{cut}, is given by $\theta_{cut} = \sqrt{\theta_s^2 + 0.12^2}$. An estimate of the number of CR background counts also passing all cuts must be made in order to determine the level of any γ-ray excess and its significance. The background counts b, were estimated using the so-called *template* model (Rowell 2003a). This model uses a subset of events normally rejected by the $\bar{w}$ cut (in this case $1.3 < \bar{w} < 1.5$), corrected for

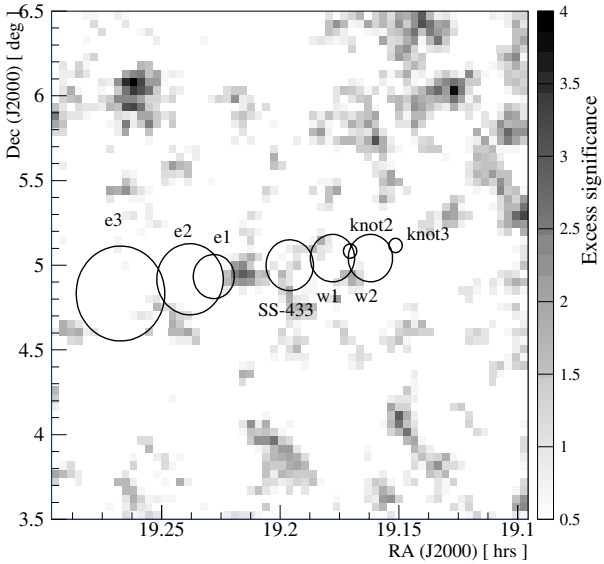

Fig. 3. Skymap of excess significance S over $3° \times 3°$ FoV, using bin steps of $0.05° \times 0.05°$. At each bin, events are integrated within a circle of $\theta_{cut} < 0.12°$, appropriate for a point source search. The locations and sizes of a-priori sources associated with SS-433 are indicated. The template background model is used to provide the CR background estimate at each bin position. Given the number of independent trials in such a skymap (of order few 100) one would expect a few $+4\sigma$ bins. See also Fig. 4.

response differences over the FoV, and yields a background estimate b spatially and temporally consistent with the source region. This was then used to estimate the excess $s - \alpha b$ for s source counts and a background normalisation α. As a check, alternative background estimates employing different spatial regions in the FoV were also implemented (e.g. regions mirrored through the tracking positions were used as background estimates). Results from these background estimates were consistent with those from the template model and are not reproduced here.

Table 3 presents the results for each a-priori location within the FoV. The statistical significance applies to an assumption of steady TeV emission throughout all observations. No convincing evidence for TeV emission was noticed at any of the a-priori source positions. Following the method of Helene (1983), 99% confidence level upper limits in the range 1 to 12% of the Crab flux were calculated. The off-axis efficiency η is taken into account when estimating all flux upper limits. Furthermore the skymaps of excess significance presented in Fig. 3 which zooms in on the SS-433 region, and Fig. 4 covering the whole FoV, show clearly that no convincing evidence for steady point-like emission is seen from any position in the FoV.

SS-433 is well known for variable and bursting output at radio to X-ray energies (see eg. Fender et al. 2000; Kotani et al. 2002), and we therefore searched for such behaviour in our dataset. In particular, regular radio outbursts are associated with jet-ejection events and a number of these have triggered X-ray observations. Our final observations were in fact triggered by the radio flare of 2 Nov. 2001 (Kotani & Trushkin 2001). In Fig. 5 we compare the daily excess significance from

Table 3. Results of a search for steady γ-ray emission at various source locations within a FoV centred near the SS-433/W50 complex. The source counts s, and the background b given by the template model, are used to estimate the excess $s - \alpha b$ and its statistical significance S. Upper limits are given at the 99% confidence level, above an energy threshold derived from the mean zenith angle of reconstructed event directions appropriate for the source region. The summed pulsar results are for those pulsars (11 in total) with predicted spin-down flux at Earth $\dot{E}/4\pi d^2 \geq 10^{-13}$ erg cm^{-2} s^{-1}.

Source	Obs. time [h]	[a] $E_{\rm th}$ [TeV]	$\theta_{\rm cut}$ [deg]	s	b	[b] S	[c] $\phi^{99\%}_{\rm crab}$ [σ]	[d] $\phi^{99\%}$
			—— SS-433/W50 and associated ——					
SS-433 *e1*	72.0	0.8	0.13	315	1972	−0.4	**0.023**	**6.18**
SS-433 *e2*	73.1	0.8	0.21	794	4980	−0.7	**0.034**	**9.18**
SS-433 *e3*	68.8	0.8	0.28	1247	8108	−2.0	**0.032**	**8.96**
SS-433	96.3	0.8	0.15	433	2541	+0.8	**0.032**	**8.93**
SS-433 *w1*	104.9	0.7	0.14	352	2168	−0.1	**0.024**	**6.65**
SS-433 *w2*	100.7	0.7	0.14	334	1994	+0.4	**0.031**	**9.00**
SS-433 knot2	103.0	0.7	0.13	271	1719	−0.6	**0.020**	**5.55**
SS-433 knot3	100.4	0.7	0.13	240	1504	−0.4	**0.023**	**6.59**
			—— Pulsars ——					
PSR J1901+0331	20.4	0.7	0.12	29	172	+0.1	**0.073**	**22.34**
PSR J1901+0413	33.3	0.7	0.12	58	362	−0.1	**0.040**	**12.86**
PSR J1901+0716	23.2	0.6	0.12	34	233	−0.6	**0.034**	**12.17**
PSR J1902+0556	38.4	0.7	0.12	131	787	+0.2	**0.031**	**10.67**
PSR J1902+06	38.4	0.7	0.12	109	759	−1.3	**0.020**	**6.93**
PSR J1902+0615	38.3	0.7	0.12	105	707	−0.9	**0.022**	**7.55**
PSR J1902+0723	23.2	0.7	0.12	40	225	+0.5	**0.064**	**22.03**
PSR J1904+0412	37.2	0.7	0.12	90	649	−1.5	**0.020**	**6.47**
PSR J1904+0800	18.8	0.6	0.12	26	100	+2.0	**0.103**	**37.37**
PSR J1905+0616	41.9	0.6	0.12	125	726	+0.5	**0.031**	**10.93**
PSR J1905+0709	41.0	0.6	0.12	76	422	+0.8	**0.034**	**12.99**
PSR J1906+0641	41.9	0.7	0.12	110	566	+1.6	**0.042**	**14.07**
PSR J1907+0345	32.9	0.7	0.12	65	443	−0.8	**0.039**	**12.24**
PSR J1907+0534	99.0	0.7	0.12	180	1178	−0.8	**0.016**	**4.75**
PSR J1907+0740	21.6	0.6	0.12	29	163	+0.4	**0.038**	**13.80**
PSR J1908+0457	96.9	0.7	0.12	165	1232	−2.5	**0.011**	**3.22**
PSR J1908+0500	96.9	0.7	0.12	176	1208	−1.4	**0.015**	**4.41**
PSR J1908+0734	21.6	0.7	0.12	35	195	+0.5	**0.053**	**18.64**
PSR J1908+0839	4.1	0.6	0.12	5	20	+0.8	**0.181**	**67.23**
PSR J1909+0254	16.9	0.7	0.12	14	157	−2.4	**0.030**	**8.92**
PSR J1909+0616	99.6	0.7	0.12	141	909	−0.6	**0.020**	**6.15**
PSR J1910+0358	76.3	0.8	0.12	148	908	−1.6	**0.028**	**7.56**
PSR J1910+0534	102.2	0.7	0.12	225	1387	−0.1	**0.022**	**6.38**
PSR J1910+0714	24.9	0.7	0.12	46	233	+1.2	**0.059**	**19.86**
PSR J1913+0446	70.7	0.8	0.12	255	1619	−0.6	**0.021**	**5.66**
PSR J1913+0832	1.9	0.6	0.12	3	38	−1.4	**0.095**	**35.55**
PSR J1915+07	10.3	0.7	0.12	22	77	+2.2	**0.098**	**33.59**
PSR J1915+0738	17.6	0.6	0.12	16	148	−1.7	**0.020**	**7.34**
PSR J1916+07	6.7	0.7	0.12	14	49	+1.7	**0.118**	**39.63**
PSR J1918+0734	4.8	0.6	0.12	7	50	−0.4	**0.070**	**27.41**
PSR J1918+08	2.9	0.6	0.12	3	18	+0.0	**0.125**	**49.34**
PSR J1926+0431	2.8	0.6	0.12	1	12	−0.8	**0.093**	**32.19**
$\sum$ Pulsars $\dot{\rm E}/(4\pi {\rm d}^2) \geq 10^{-13}$	495.3	0.7	0.12	1109	6724	+0.4	**0.007**	**2.15**
			—— SNR ——					
SNR 039.2-00.3 (3C 396)	45.1	0.7	0.133	187	1176	−0.4	**0.025**	**8.46**
SNR 040.5-00.5	51.6	0.7	0.219	334	2016	+0.2	**0.048**	**16.11**
SNR 041.1-00.3 (3C 397)	27.8	0.7	0.12	56	338	+0.1	**0.038**	**13.20**
			—— Others ——					
GeV J1907+0557	87.0	0.7	0.12	172	969	+1.0	**0.026**	**8.55**
AXJ1907.4+0549	98.5	0.7	0.12	174	1054	+0.1	**0.021**	**6.29**

[a] Estimated γ-ray threshold energy for mean zenith $\bar{z}$: $E_{\rm th} = 0.5\cos(\bar{z})^{-2.5}$.
[b] Statistical significance using Eq. (17) of 1983, Norm. factor $\alpha = 0.163$.
[c] $\phi^{99\%}_{crab}$ = 99% upper limit in units of Crab flux, (1 Crab = 1.75×10^{-11} ph cm^{-2} s^{-1} (Aharonian et al. 2000).
[d] $\phi^{99\%}_{ph}$ = 99% upper limit for $E > E_{\rm th}$ ($\times 10^{-13}$ ph cm^{-2} s^{-1}).

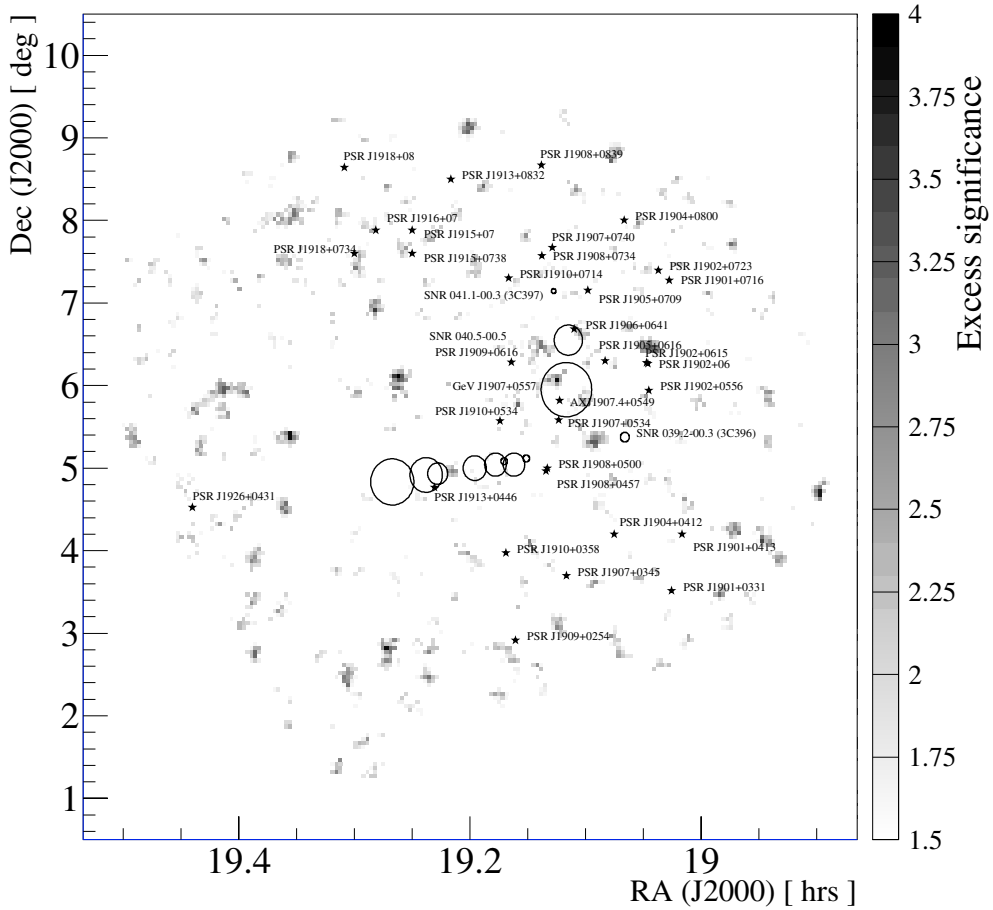

Fig. 4. Skymap of excess significance S (only values $S \geq 1.5$ are shown) over an ~8° × 8° FoV, using bin steps of 0.05° × 0.05°. At each bin, events are integrated within a circle of $\theta_{\rm cut} < 0.12°$, as for Fig. 3. The locations of a-priori sources are indicated (Pulsars indicated as a star; SNR indicated by circular approximations to their sizes; GeV J1907+0557 is represented by its location error circle, and includes the ASCA source AXJ1907.4+0549). The template model is used to provide the CR background estimate at each bin position. The 1D distribution of significances of this skymap (within $\pm 5\sigma$) is well fitted by a Gaussian of mean $\mu = 0.106 \pm 0.007$ and std. dev $\sigma = 1.012 \pm 0.005$. SS-433 and associated objects are represented by the central group of circles.

HEGRA IACT-System events consistent with the SS-433 direction (within $\theta < 0.12°$), with the X-ray (RXTE ASM) and radio light curves (Green Bank Interferometer (GBI)[2] and RATAN 600) for the period encompassing our observations. No significant excess on a nightly basis is seen in our observations, which often overlap and closely follow the radio outbursts seen in the publically-available GBI and RATAN 600 (Trushkin 2004; see also Trushkin et al. 2003) data. As a guide, the 5σ sensitivity of the HEGRA IACT-System achieved on a nightly basis is between 0.35 and 0.50 Crab flux ($E > 0.8$ TeV) or 1.24 to 1.77 ($\times 10^{-11}$ erg cm^{-2} s^{-1}) given that between 1 to 2 h exposure are obtained per night on SS-433.

As a further, more general test for variability over the entire FoV, we implemented the powerful *exp-test* described by Prahl (1999). The *exp-test* is based on whether event arrival times deviate from a Poisson process. This generally requires detailed knowledge of, and correction for the temporal response function of the instrument. However, background events are also concurrently accumulated, and can be used as an in-situ measure of the temporal response. The *exp-test* may therefore be constructed by forming the distribution of the number of background events between successive γ-ray like events. In this way the *exp-test* requires no event times, no normalisation, and data gaps are automatically taken into account. For binned positions in the FoV, the γ-ray-like events ($\bar{w} < 1.1$) and background events ($1.3 < \bar{w} < 1.5$, from the template model) are accumulated in a single pass over data, and the *exp-test* significance $S_{\rm exp}$ calculated. The skymap of *exp-test* significances obtained from all data is presented in Fig. 6. $S_{\rm exp}$ can be expressed as a function of the assumed duty cycle q, the ratio of high to low flux states r and the number of events used in each bin $N = s + b$ (see Eq. (44) of Prahl 1999). The measured $S_{\rm exp}$ value at each point in the FoV, and its corresponding N value can therefore be used to constrain a locus of duty cycle r vs. q values (Fig. 5 of Prahl 1999). As an example, for the SS-433 region (and others in the central 3 to 4 degrees) the constraint $S_{\rm exp} =< 0.1\sqrt{N}$ (as per Fig. 5 of Prahl 1999) rules out flux ratios $r > 2.0$ for duty cycles $q = 0.2$ to 0.8 (corresponding to variability on timescales of ~20 to 80 h given the ~100 h total exposure).

[2] The GBI was a facility of the USA National Science Foundation operated by the NRAO in support of NASA High Energy Astrophysics programs.

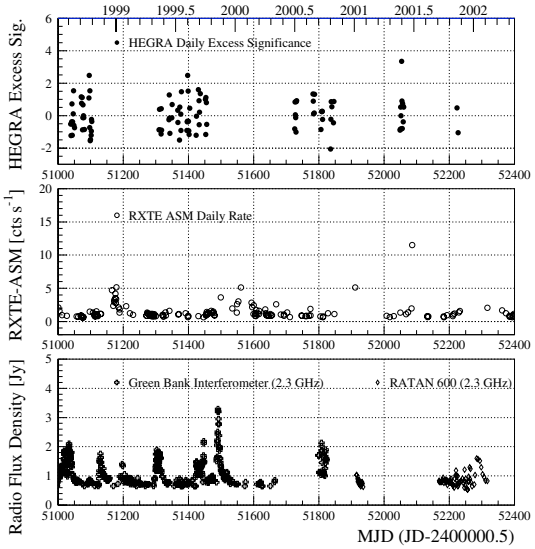

Fig. 5. For the SS-433 region: comparison of the daily excess significance from HEGRA IACT-System data, X-ray (RXTE ASM) and radio (Green Bank Interferometer and RATAN 600) light curves.

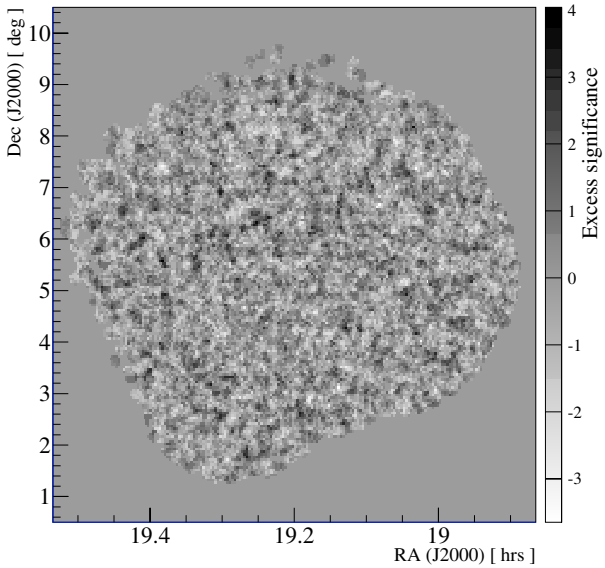

Fig. 6. Skymap of *exp-test* significance from Prahl (1999) over the FoV (range and binning are the same as in Fig. 4 using the entire dataset. The 1D distribution of significances is well fitted by a Gaussian of mean $\mu = 0.024 \pm 0.0007$ and std. dev. $\sigma = 0.965 \pm 0.005$.

4. Discussion and conclusions

We have performed a search for TeV γ-ray emission from SS-433 and associated objects, 23 pulsars, three SNR and the unidentified EGRET source GeV J1907+0557 with the HEGRA IACT-System. No evidence for steady or variable TeV emission has been seen and we discuss here some implications of the upper limits obtained.

Concerning the *e3* region of SS-433, the inverse-Compton emission predicted by AA lies in the range 10^{-12} to 10^{-11} erg cm^{-2} s^{-1}. The radio spectral index at $\alpha \sim 0.5$ (Downes et al. 1986) (a value of $\alpha \sim 0.68$ is calculated by

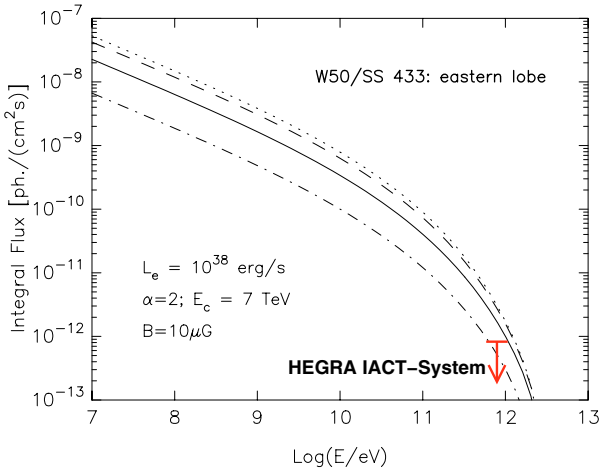

Fig. 7. Integral flux of inverse-Compton emission expected from the SS-433/W50 eastern lobe *e3* region for different source radii (Aharonian & Atoyan 1998): 0.1° (dot-dashed), 0.25° (solid, actual radio "ear" size), 0.5° (dashed) and 2.0° (dotted). Our upper limit is included and assumes a source radius of 0.25° (ie. to be compared with the solid line). The increasing predicted flux with opening angle results from the fact that the IC emission is actually emitted over a considerably wider solid angle, reflecting the ubiquitous nature of the CMB target photon field.

Dubner 2000; see also Dubner et al. 1998) and spatial correlation of the radio and X-ray fluxes support the notion that diffusive shock acceleration of electrons to TeV energies is taking place at *e3*. AA find that an electron injection spectrum of the form $N(E) \sim E^{-2}\exp(-E/7\ \mathrm{TeV})$ fits the radio and X-ray fluxes well. Determination of the electron injection rate is linked to the B-field (in this model, considered a free parameter) since the radio flux $\propto B^{1.5}L_e$ where L_e (erg s^{-1}) is the injection power of electrons. AA also consider a number of source sizes, concluding that the measured size of the radio lobe corresponding to *e3*, of radius ~0.25°, is consistent with a diffusion coefficient implied from cosmic-ray flux transport in the galactic disk. A comparison of our upper limit for *e3* $F(E > 0.8\ \mathrm{TeV}) < 8.93 \times 10^{-13}$ ph cm^{-2} s^{-1} with the predictions of AA (for various source sizes) is presented in Fig. 7. Our upper limit constrains somewhat the prediction of AA assuming a source radius of 0.25°, a B-field of 10 μG, and injection rate of $L_e = 10^{38}$ erg s^{-1}. Using the direct relationship between the expected IC (f_γ) and X-ray energy fluxes (f_x) arising from the *same* electrons (Eq. (1)) we can establish a condition on the post-shocked magnetic field B of the *e3* region. The mathematical caveat here is that the corresponding energy range in the TeV and keV regimes must be adhered to and that we assume that the emission regions of both components have the same size as in the model of AA. The IC (E TeV) and X-ray (ϵ keV) synchrotron energies in Eq. (1) are coupled according to Eq. (2) (Aharonian et al. 1997), so that a comparison of the γ-ray energy flux f_γ in the range $E \sim 0.8$ to 10 TeV with the X-ray energy flux in the range $\epsilon \sim 0.1$ to 2.4 keV (L_x(0.1–2.4 keV) ~2.3×10^{35} erg s^{-1} or 6.35×10^{-11} erg cm^{-2} s^{-1} at 5.5 kpc) will yield an appropriate value of $B \sim 10$ to 100 μG expected after shock compression. In estimating f_γ we also assumed a differential photon index of −3.7 which is the same as that for

the X-ray emission. According to Eq. (1) we therefore derive a *lower limit* on the magnetic field within *e3* of $B \geq 19\ \mu$G. This B limit is consistent with the equipartition field for *e3* estimated at $B \sim 20$ to 60 μG (Safi-Harb & Ögelman 1997, using a source region of radius ~25 pc, or ~0.25° at 5.5 kpc). We do not discuss further results for the other regions along the jets (e1, e2, w1, w2, knot2, knot3) since no predictions for TeV γ-ray fluxes are available. Given however the strong non-thermal X-ray fluxes for e1 and e2, one could also constrain the B field in these regions using our upper limits.

For the 32 pulsars that are within our survey FoV, our null results might be expected since the emission arising from within the outer magnetosphere according to the polar cap and outer gap models would likely fall-off very steeply in the $E < 50$ GeV energy regime. Extra high energy components extending to the TeV regime under the outer gap model (inverse-Compton emission extending to $E > 1$ TeV Hirotani et al. 2001) and unshocked wind models (Aharonian & Bogovalov 2003) are however predicted. Our results can be used to examine in general the overall energy available for very high energy γ-ray emission, which could arise for example from a pulsar wind nebula (see for e.g. Aharonian et al. 1997). Based on the source stacking method outlined in Aharonian et al. (2002) we considered combined results from a subset of pulsars selected according their predicted spin-down flux observed at Earth $\dot{E}_{\rm d} \sim \dot{E}/(4\pi d^2) \geq 10^{-13}$ erg cm^{-2} s^{-1} where the distance d is estimated from the pulsar's dispersion measure (DM). The spin-down flux $\dot{E}_{\rm d}$ for each pulsar has been taken from the online ATNF catalogue[3]. A total of 11 pulsars of our sample meet this condition and their average $\dot{E}_{\rm d}$ at Earth, weighted according to effective exposure (ηt), is 4.74×10^{-12} erg cm^{-2} s^{-1} (or 4.9×10^{-6} Crab spin-down flux units). Our upper limit at 2.15×10^{-13} erg cm^{-2} s^{-1} therefore implies that on average no more than 4.5% of a pulsar's spin-down flux is available for γ-ray production at energies $E > 0.7$ TeV (Note this is a considerably larger fraction than that observed for the Crab where the flux $E > 1$ TeV is $\sim 10^{-5}\dot{E}_{\rm d}$). The source stacking method assumes also that each of these 11 pulsars would convert the same fraction of their spin-down flux into TeV γ-ray production.

Turning to other potential TeV sources in our FoV, Olbert et al. (2003) discuss recent Chandra observations of the composite SNR 3C 396, revealing strong evidence for a central pulsar wind nebula. Taking their derived total spin-down luminosity of the putative central pulsar at 7.2×10^{36} erg s^{-1}, and conservative distance estimate of 9.6 kpc, our upper limit implies a maximum 0.01% of the spin-down power would be converted into TeV γ-rays. With a suitable model, this could then be used to constrain the post-shocked B field under the synchrotron/inverse-Compton scenario, similar to that discussed earlier for the SS-433 *e3* region. 3C 397, studied at length by Safi-Harb et al. (2000), is a composite SNR with centre-filled X-ray morphology and shell radio morphology. It is in fact one of the brightest SNR at radio energies. The broad-band X-ray results ROSAT, ASCA and RXTE have been interpreted in both young ejecta-dominated and older Sedov phase scenarios. The X-ray spectrum is line-dominated and thermal in origin but an extra component attributed to a pulsar-driven process is not ruled out at present. Our upper limit may provide useful constraints on any S/IC emission expected, as for 3C 396. The remaining SNR of our survey, SNR 040.5-00.5 (Downes et al. 1980) has been linked to the EGRET source 3EG J1903+0550 (Bhattacharya et al. 2003).

ASCA X-ray follow-up observations of the EGRET GeV catalogue of Lamb & Macomb (1997) revealed a possible counterpart, AXJ1907.4+0549, to the catalogued GeV source in our FoV, GeV J1907+0557 (Roberts et al. 2001). We finalise in this paper the preliminary HEGRA results for these two objects outlined by Rowell et al. (2003b), and find no evidence for point-like TeV emission from either position.

We eagerly await future observations of SS-433 and the surrounding field with the next generation of ground-based instruments such as H.E.S.S, VERITAS, CANGAROO-III and MAGIC (Hofmann et al. 2003; Weekes et al. 2002; Kubo et al. 2004; Lorenz et al. 1999).

Acknowledgements. The support of the German ministry for Research and technology BMBF and of the Spanish Research Council CICYT is gratefully acknowledged. We thank the Instituto de Astrofísica de Canarias for the use of the site and for supplying excellent working conditions at La Palma. We gratefully acknowledge the technical support staff of the Heidelberg, Kiel, Munich, and Yerevan Institutes. G.P.R. acknowledges receipt of a von Humboldt fellowship.

[3] ATNF Pulsar Catalogue
http://www.atnf.csiro.au/research/pulsar/psrcat/

References

Aharonian, F. A., & Bogovalov, S. V. 2003, New Astron., 8, 85
Aharonian, F. A., Atoyan, A. M., & Kifune, T. 1997, MNRAS, 291, 162
Aharonian, F. A., & Atoyan, A. M. 1998, New Astron. Rev., 42, 579
Aharonian, F. A., Akhperjanian, A. G., Barrio, J. A., et al. 2000, ApJ, 539, 317
Aharonian, F. A., Akhperjanian, A. G., Beilicke, M., et al. 2002, A&A, 395, 803
Band, D. L., & Grindlay, J. E. 1986, ApJ, 311, 595
Bhattacharya, D., Akyüz, A., Miyagi, T., et al. 2003, A&A, 404, 163
Blandford, R. D. & Ostriker, J. P. 1980, ApJ, 237, 808
Brinkmann, W., Aschenbach, B., & Kawai, N. 1996, A&A, 312, 306
Downes, A. J. B., Pauls, T., & Salter, C. J. 1980, A&A, 92, 47
Downes, A. J. B., Pauls, T., & Salter, C. J. 1986, MNRAS, 218, 393
Dubner, G. M. 2000, priv. comm.
Dubner, G. M., Holdaway, M., Goss, W. M., & Mirabel, I. F. 1998, AJ, 116, 1842
Fender, R., Rayner, D., Norris, R., et al. 2000, ApJ, 530, L29
Fuchs, Y. 2002, in Proc. The Gamma-Ray Universe, XXIInd Moriond Astrophysics Meeting, Les Arcs, Savoie, France, March 9–16 [arXiv:astro-ph/0207429]
Fuchs, Y., Koch-Miramond, L., & Ábrahám, P. 2002, Proc. 4th Microquasar Workshop, ed. Ph. Durouchoux, Y. Fuchs, & J. Rodríguez [arXiv:astro-ph/0208432]
Hayashi, S., Kajino, F., Naito, T., et al. 2003, Proc. 28th ICRC Tsukuba OG2, 2533

Hillas, A. M. 1985, in Proc. 19th ICRC, 3, 449
Hirotani, K. 2001, ApJ, 549, 495
Hofmann, W., Jung, I., Konopelko, A., et al. 1999, Astropart. Phys., 12, 135
Hofmann, W., et al. 2003, in Proc. 28th ICRC Tsukuba Japan
Helene, O. 1983, Nucl. Inst. Meth., 212, 319
Kawai, N., & Kotani, T. 1999, Astron. Nachr., 320, 211
Kotani, T., & Trushkin, S. 2001, IAU Circ., 7747, 7748
Kotani, T., Trushkin, S., & Denissyuk, E. K. 2002, Proc. 4th Microquasar Workshop, ed. Ph. Durouchoux, Y. Fuchs, & J. Rodríguez [arXiv:astro-ph/0208250]
Kubo, H., Asahara, A., & Bicknell, G. V. 2004, New Astron. Rev., 48, 485
Lamb, R. C., & Macomb, D. J. 1997, ApJ, 488, 872
Li, T., & Ma, Y. 1983, ApJ, 272, 317
Lorenz, E. 1999, in Proc. Towards a Major Atmospheric Cherenkov Detector – VI, ed. B. L. Dingus, M. H. Salamon, & D. B. Kieda, AIP Conf. Ser., 515, 510
Margon, B. 1981, Science, 215, 247
Margon, B. 1984, ARA&A, 22, 507
Mirabel, I. F., & Rodríguez, L. F. 1999, ARA&A, 37, 409
Olbert, C. M., Keohane, J. W., Arnaud, K. A., et al. 2003, ApJ, 592, L45
Prahl, J. 1999 [arXiv:astro-ph/9909399]
Pühlhofer, G., Bolz, O., Götting, N., et al. 2003, Astropart. Phys., 20, 267
Roberts, M., Romani, R. W., & Kawai, N. 2001, ApJS, 133, 451
Rowell, G. P. 2000, in Proc. Similarities and Universality in Relativistic Flows (Berlin: Logos Verlag), Mykonos, Greece, ed. M. Georganopoulos, A. Guthmann, K. Manolakou, & A. Markowith [arXiv:astro-ph/0104288]
Rowell, G. P. 2001, in Proc 27th ICRC Hamburg OG157 http://www.copernicus.org/icrc/OG2.02.post.htm
Rowell, G. P. 2003a, A&A, 410, 389
Rowell, G. P. 2003b, in Proc 28th ICRC Tsukuba OG2.2, 2329 http://www-rccn.icrr.u-tokyo.ac.jp/icrc2003/PROCEEDINGS/PDF/575.pdf
Safi-Harb, S., & Ögelman, H. 1997, ApJ, 483, 868
Safi-Harb, S., & Petre, R. 1999, ApJ, 512, 784
Safi-Harb, S., Petre, R., Arnaud, K. A., et al. 2000, ApJ, 545, 922
Trushkin, S. A., Bursov, N. A., & Nizhelskij, N. A. 2003, Bull. Spec. Astrophys. Obs., 56, 57 [arXiv:astro-ph/0403037]
Trushkin, S. A. 2004, RATAN 600 Online Monitoring Data http://cats.sao.ru/šatr
Vermeulen, R. C., Schilizzi, R. T., Spencer, R. E., et al. 1993, A&A, 270, 177
Weekes, T. C., Badran, H., Biller, S. D., et al. 2002, Astropart. Phys., 17, 221